

# In Situ TEM Observations of $\text{Cu}_6\text{Sn}_5$ Polymorphic Transformations in Reaction Layers Between Sn-0.7Cu Solders and Cu Substrates

K. NOGITA<sup>1,5</sup>, M.A.A. MOHD SALLEH<sup>1,2</sup>, E. TANAKA<sup>3</sup>, G. ZENG<sup>1</sup>,  
S.D. MCDONALD<sup>1</sup> and S. MATSUMURA<sup>3,4</sup>

1.—Nihon Superior Centre for the Manufacture of Electronic Materials (NS CMEM), School of Mechanical and Mining Engineering, The University of Queensland, St Lucia, Brisbane, QLD 4072, Australia. 2.—Centre of Excellence Geopolymer and Green Technology, School of Materials Engineering, Universiti Malaysia Perlis (UniMAP), Taman Muhibbah, 02600 Jejawi, Arau, Perlis, Malaysia. 3.—The Ultramicroscopy Research Center, Kyushu University, Fukuoka 819-0395, Japan. 4.—Department of Applied Quantum Physics and Nuclear Engineering, Kyushu University, Fukuoka 819-0395, Japan. 5.—e-mail: k.nogita@uq.edu.au

Direct evidence of the relationship between the polymorphic phase transformation from monoclinic  $\text{Cu}_6\text{Sn}_5$  to hexagonal  $\text{Cu}_6\text{Sn}_5$  and stress accumulation/release in  $\text{Cu}_6\text{Sn}_5$ , formed at the interface between Sn-0.7Cu lead-free solder and their Cu substrates, has been obtained. To explore this challenging phenomenon, we developed an in situ heating/isothermal observation technique in ultrahigh-voltage transmission electron microscopy that enables the observation of thick samples (around 0.5  $\mu\text{m}$ ) for solder joints, including Cu/ $\text{Cu}_3\text{Sn}$ / $\text{Cu}_6\text{Sn}_5$ /Sn-0.7Cu solder interfaces prepared by a focused ion beam milling technique. The results show evidence of stress creation and release events by imaging bend contours that may arise due to the polymorphic transformations of the  $\text{Cu}_6\text{Sn}_5$  phase and the associated volumetric change.

## INTRODUCTION

During the transition from traditional to lead-free soldering, there has been a simultaneous increase in the complexity and spatial density of electrical packages (combined circuitry/chips/solder, etc.). This miniaturization of circuitry has resulted in proportionally smaller volumes of solder at electrical interconnects.<sup>1</sup> In the past, a solder joint would retain a significant layer of the original Sn-alloy solder (Sn-0.7 wt.%Cu, for example). The drive toward miniaturization has resulted in a relative increase in the volume fraction of intermetallic compounds (IMCs) in the microstructure of solder joints, and in some cases, a solder joint may consist almost entirely of  $\text{Cu}_6\text{Sn}_5$  and  $\text{Cu}_3\text{Sn}$ <sup>2</sup> with different mechanical and physical properties and the coefficient of thermal expansion (CTE).<sup>3</sup> Therefore, the current understanding of the “bulk” properties of solder joints mainly consisting of the  $\beta$ -Sn phase (which is already limited for many alloy/substrate combinations) is not always relevant when designing high-performance, three-dimensional (3D)

integrated circuit (IC) electrical packages. For this reason, there is a strong and urgent need to understand (I) the growth crystallography, morphology, and anisotropic thermomechanical properties of intermetallic joints; and (II) the impact these factors have on the integrity of solder joints for micro-electronics applications. Researchers hope to use this information to develop interconnects with IMCs optimized for crack resistance.

The reaction products in solder joints are typically the IMCs  $\text{Cu}_6\text{Sn}_5$  and  $\text{Cu}_3\text{Sn}$ , often of complex crystal structures and including trace elements from both the substrate and the solder. Although conventional Sn-Cu binary phase diagrams (Fig. 1)<sup>4,5</sup> show two polymorphs of  $\text{Cu}_6\text{Sn}_5$ , up to five variants have now been identified ( $\eta$ ,  $\eta'$ ,  $\eta^6$ ,  $\eta^8$ , and  $\eta^{4+1}$ )<sup>6,7</sup> but limited information exists for these structures, in particular, for the latter three. It has been shown that a polymorphic transformation from hexagonal  $\eta$ - $\text{Cu}_6\text{Sn}_5$  to monoclinic  $\eta'$ - $\text{Cu}_6\text{Sn}_5$  occurs as the temperature falls below 186°C. We have previously shown<sup>5,8,9</sup> that the faceted eutectic  $(\text{Cu},\text{Ni})_6\text{Sn}_5$  intermetallics containing Ni remain

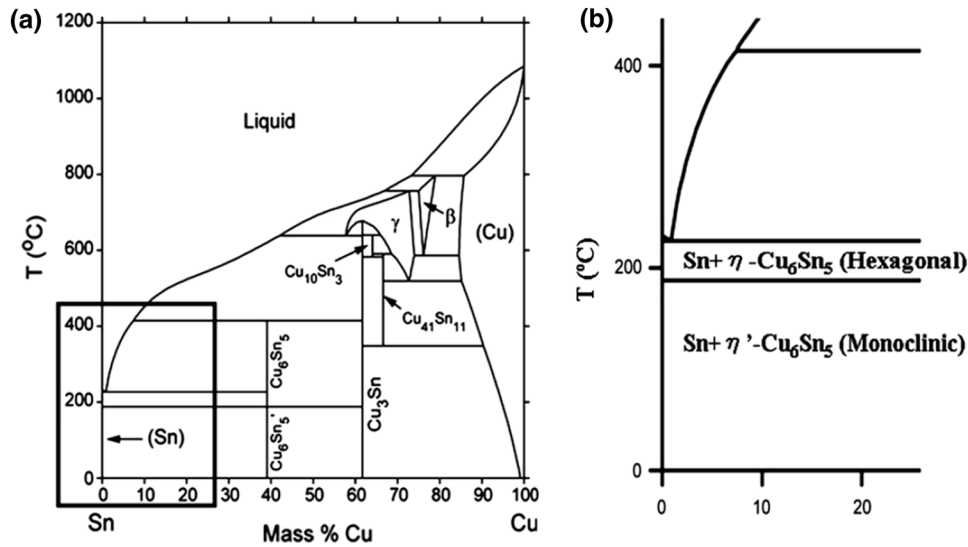


Fig. 1. (a) Sn–Cu phase diagram and (b) magnified from Sn-rich corner of (a), adapted from Refs. 4 and 5.

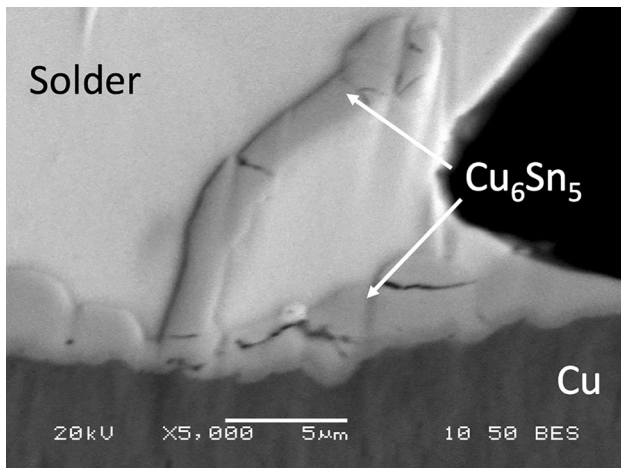


Fig. 2. A typical cross-sectioned ball grid array (Sn-0.7wt.%Cu solder) on Cu substrate, adapted from Ref. 10.

stable in the hexagonal  $\eta$  phase at room temperature when, in contrast, identically cooled binary  $\text{Cu}_6\text{Sn}_5$  transform into the low-temperature monoclinic  $\eta'$  phase. This discovery is important as the transformation is associated with a volumetric change, and this has been hypothesized to be a cause of internal stress generation in soldered joints during real-world applications. Research has already led to improvements in the performance of this IMC layer.<sup>3</sup> Nogita et al.<sup>10</sup> shows an example of a ball grid array (BGA) soldered joint (see Fig. 2), commonly used in mobile phones and e-tablets, on an electronic circuit board produced using a slightly hypo-eutectic lead-free solder alloy (Sn-0.7Cu), which has a microstructure consisting of Sn primary dendrites and Sn- $\text{Cu}_6\text{Sn}_5$  eutectic. The cross section of the IMC layer between the solder ball and the Cu substrate contains  $\eta$  crystals of  $\text{Cu}_6\text{Sn}_5$ , and

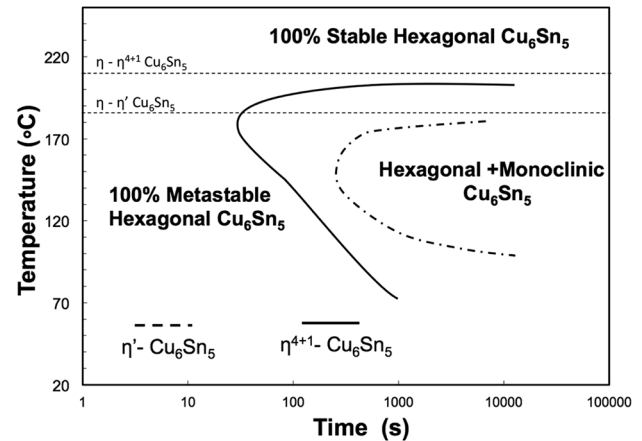


Fig. 3. Schematic TTT diagrams of hexagonal to monoclinic transformations in  $\text{Cu}_6\text{Sn}_5$  intermetallics, adapted from Refs. 11 and 12.

within these crystals are cracks and voids that are generated during solidification and cooling to room temperature.<sup>10</sup> These cracks compromise the reliability and diminish the shock resistance of the final microelectronic devices. By adding trace Ni additions to this solder, we demonstrated that the  $\text{Cu}_6\text{Sn}_5$  layer becomes stabilized in the hexagonal polymorph, undergoes less cracking, and the growth texture of the layer is altered.<sup>10</sup> Nevertheless, direct evidence between the polymorphic phase transformations and the generation of stress has yet to be provided. Additionally, although time–temperature–transformation (TTT) diagrams of monoclinic to hexagonal transformations have been developed (see Fig. 3),<sup>11,12</sup> detailed mechanisms of the polymorphic phase transformation, such as nucleation and growth of monoclinic to hexagonal  $\text{Cu}_6\text{Sn}_5$ , in real solder joints (Cu/ $\text{Cu}_3\text{Sn}$ / $\text{Cu}_6\text{Sn}_5$ /Sn-0.7Cu solder), is not known.

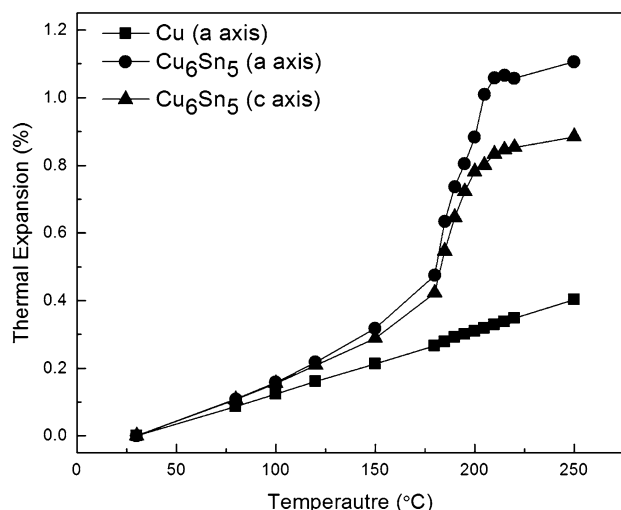


Fig. 4. Whole-pattern profile fitting method to determine thermal expansion behavior of interfacial  $\text{Cu}_6\text{Sn}_5$  and Cu substrate. The variation in lattice parameters of  $\text{Cu}_6\text{Sn}_5$  and Cu in the temperature range 30–250°C, adapted from Ref. 20.

A significant challenge in research on the link between phase transformation and crack formation has been the difficulty of proving the cracking mechanisms, and therefore, the mechanisms have long been the subject of questions. As a result, so far we proposed three possible hypotheses for the cause of cracking of  $\text{Cu}_6\text{Sn}_5$ <sup>10</sup> as (I) polymorphic transformations and associated stresses;<sup>5,8,9</sup> (II) mismatch of mechanical properties, such as hardness and elastic modulus between interfacial structures;<sup>13–15</sup> and (III) growth orientations associated with anisotropy of mechanical properties.<sup>15–19</sup> This lack of fundamental understanding is reflected in many solder alloys and hampers the further rational development of alloys for increased reliability and use in emerging and demanding applications such as 3D ICs.

As shown in Fig. 4, we have performed in situ x-ray diffraction (XRD) heating experiments<sup>20</sup> to determine the thermal expansion behavior of interfacial  $\text{Cu}_6\text{Sn}_5$  and Cu substrates with Sn-0.7 wt.%Cu solder. In addition to the difference of the thermal expansion between  $\text{Cu}_6\text{Sn}_5$  and Cu, there is a large discontinuity between them at around 180°C, which corresponds to the volume change due to the polymorphic transformation from monoclinic  $\text{Cu}_6\text{Sn}_5$ . In situ transmission electron microscopy (TEM) is an established experimental technique that permits direct observation of the dynamics and mechanisms of deformation behavior. In this article, we report on direct evidence for the relationship between the polymorphic phase transformation and stress accumulations/release in  $\text{Cu}_6\text{Sn}_5$  by using ultrahigh-voltage transmission electron microscopy (UHV-TEM) with controlled temperature in situ observations.

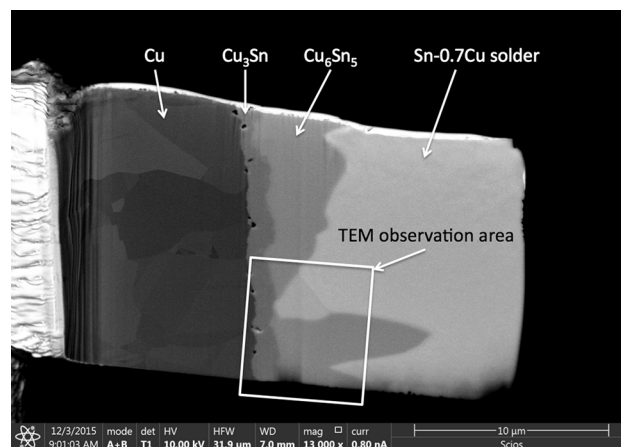


Fig. 5. SEM image of the sample. Area showing corresponds to the in situ observation with heating and isothermal.

## EXPERIMENTAL PROCEDURES

### BGA-Sample Preparation

Sn-0.7 wt.%Cu bulk alloy was first prepared by casting a mixture of Sn and Cu. The solidified bulk sample was then cut into thin sheets, and its composition was confirmed by using energy-dispersive x-ray spectroscopy (EDS) to be in the range of 99.3 wt.% Sn and 0.7 wt.% Cu. Sn-0.7 wt.%Cu solder sheets were further rolled at room temperature to approximately 0.02 mm thickness. The thinned sheets were then punched into 2.5-mm-diameter disks and further heated on a Pyrex plate to 250°C with the aid of  $\text{N}_2$  gas flow to form a ball shape. The fabricated solder balls were then sieved to achieve spheres of 500–600  $\mu\text{m}$ . The solder balls, with a small amount of rosin mildly activated (RMA) flux, were then soldered onto a Cu with an organic soldering preservative surface finish (Cu-OSP) printed circuit board (PCB) with a 600- $\mu\text{m}$  ball pitch using a tabletop reflow oven with a maximum 250°C reflow temperature and 127-s reflow time with  $\text{N}_2$  gas flow. The solder joint samples were then further annealed for 500 h at 150°C.

### UHV-TEM Sample Preparations

Annealed samples were cross-sectioned and fine polished perpendicular to the solder/Cu interface. UHV-TEM samples were then prepared by using a FEI SCIOS focus ion beam (FIB) dual beam system. This system was used with the electron and ion column mounted at 52° to each other on a 21-port specimen chamber and a 7-mm working distance; the featured area perpendicular to the solder/Cu interface was deposited with a Pt protective layer approximately 1.5  $\mu\text{m}$  thick. By using a 30-nA and 15-nA beam, two cross sections were milled in serial mode to provide a 2- $\mu\text{m}$  lamella. Then, by using the Easylift needle tip, the lamella cross-sectioned sample was transferred and welded with Pt deposition on a Cu TEM grid. Finally, to provide a

smooth cross-section area for UHV-TEM observation, the welded samples were thinned to about  $0.5 \mu\text{m}$  thickness by using  $0.5\text{-nA}$  beam current. Figure 5 shows scanning electron microscopy (SEM) images of the sample, which clearly shows the cross-sectioned Cu/Cu<sub>3</sub>Sn/Cu<sub>6</sub>Sn<sub>5</sub>/Sn-0.7Cu solder. The area shown in Fig. 5 corresponds to the in situ observation area.

### In Situ Synchrotron XRD Characterization

For XRD experiments, Sn-0.7Cu/Cu solder joints were prepared by dipping Cu plates (C1220P) of  $10 \text{ mm} \times 30 \text{ mm} \times 0.3 \text{ mm}$  with flux into the molten solder in a solder bath at  $270^\circ\text{C}$ . Samples were etched after being annealed for 500 h at  $150^\circ\text{C}$  in a solution of ortho-nitrophenol (35 g) and NaOH (50 g) in 1 L of water at  $80^\circ\text{C}$  to completely remove the Sn phase from the solder alloys. XRD data were obtained from the prepared dipped Sn-0.7Cu/Cu

samples at  $30^\circ\text{C}$ ,  $150^\circ\text{C}$ , and  $250^\circ\text{C}$ , in flat-plate asymmetric reflection geometry with sample heater at the powder diffraction beamline of the Australian Synchrotron by using an x-ray energy of 18 keV. The wavelength ( $0.689 \text{ \AA}$ ) and  $2\theta$  zero-error were determined from a standard  $0.3\text{-mm}$  capillary of a LaB<sub>6</sub>/Si mixture by using transmission geometry. The angle between the x-ray beam and the sample surface was fixed at  $5^\circ$ . Indexing of XRD patterns was conducted with TOPAS 4.2 software. A fundamental parameter (FP) approach was employed in TOPAS.<sup>21</sup>

### In Situ UHV-TEM Observations

In situ UHV-TEM observations were performed with a JEM-1000 (JEOL, Japan) at an acceleration voltage of 1000 kV with an EM-HSTH (JEOL, Japan) heating holder and high-resolution video recorder. Figure 6 shows the temperature profile

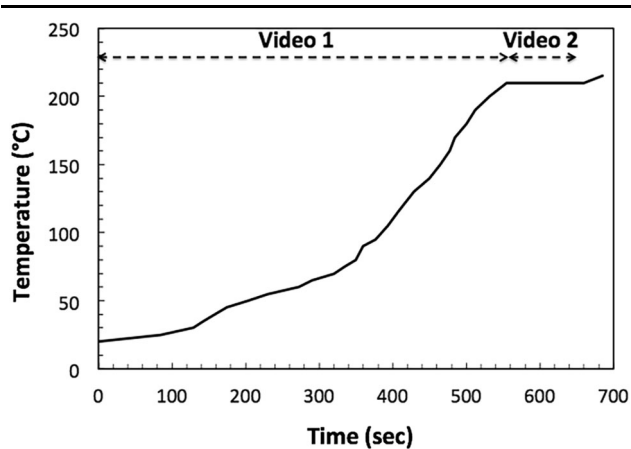


Fig. 6. Temperature profile for the in situ observation of the sample.

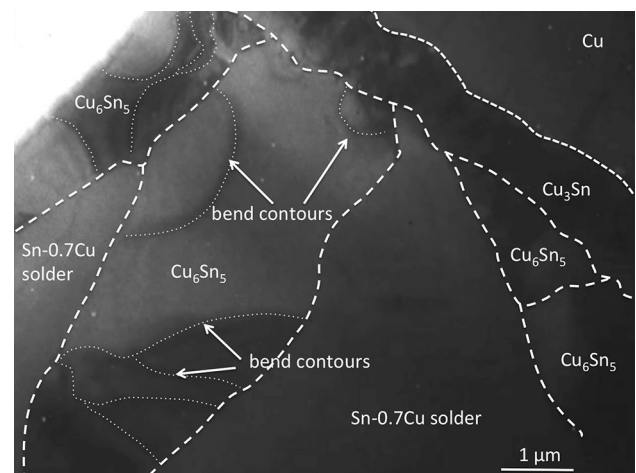


Fig. 8. Still-frame TEM images from in situ video of an interface in Cu/Cu<sub>3</sub>Sn/Cu<sub>6</sub>Sn<sub>5</sub>/Sn taken at  $210^\circ\text{C}$ .

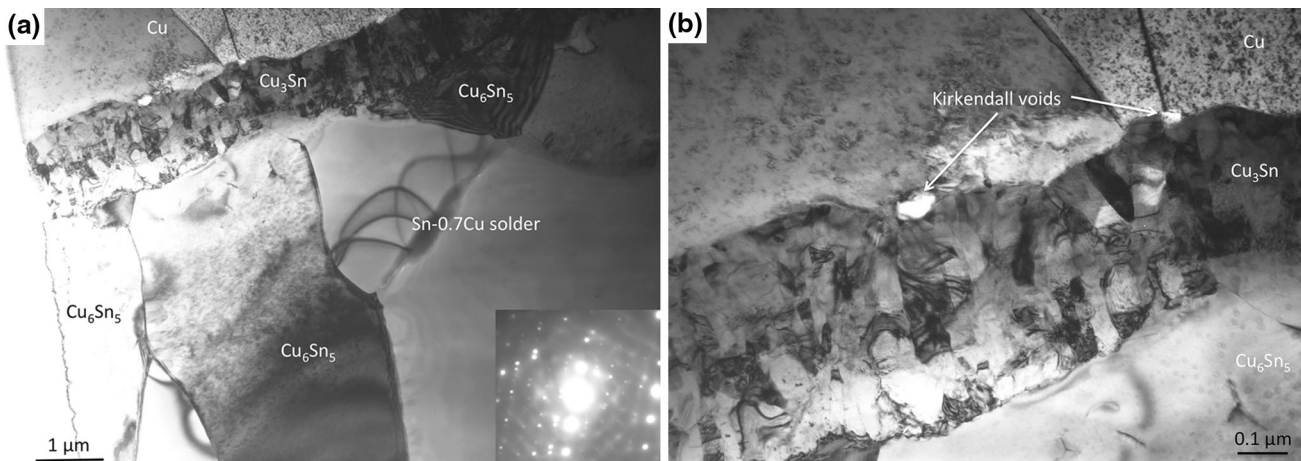


Fig. 7. (a) Low-magnification bright field image of solder joint with selected area electron diffraction from Cu<sub>6</sub>Sn<sub>5</sub>, and (b) high-magnification bright field image of Cu/Cu<sub>3</sub>Sn/Cu<sub>6</sub>Sn<sub>5</sub> interface.

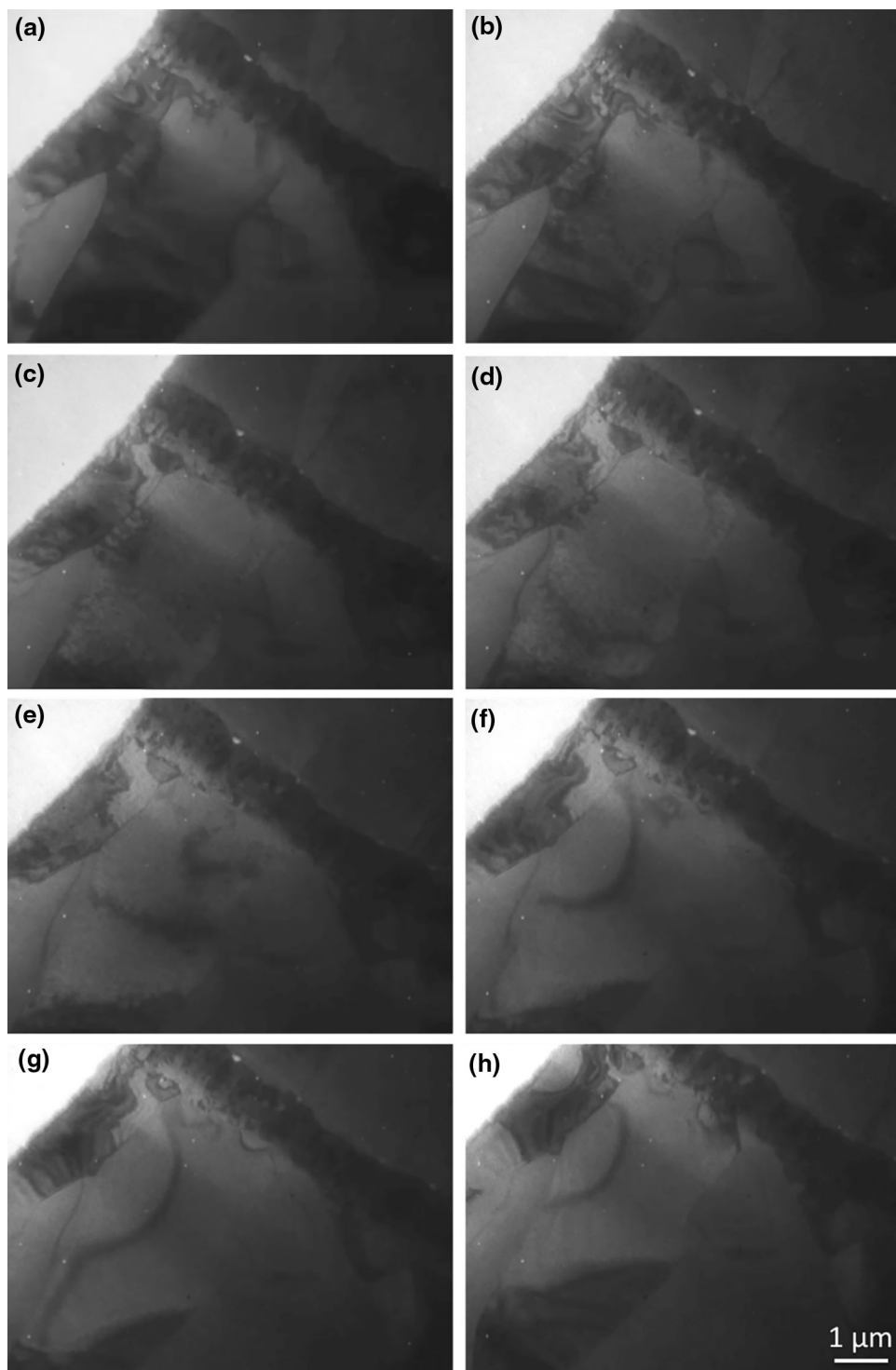


Fig. 9. Selected still-frame TEM images from in situ video of high-voltage TEM of an interface in  $\text{Cu}/\text{Cu}_3\text{Sn}/\text{Cu}_6\text{Sn}_5/\text{Sn}$  taken at (a) 20°C, (b) 60°C, (c) 120°C, (d) 150°C, (e) 180°C, (f) 190°C, (g) 200°C, and (h) 210°C.

for the in situ observation of the sample. A sample was measured at room temperature and then heated from 25°C to 210°C with a heating rate of approximately 20°C/min following isothermal

observations at 210°C. The beam-induced heating remains small at the acceleration voltage of 1000 kV, allowing for proper observations of the phase transformation.

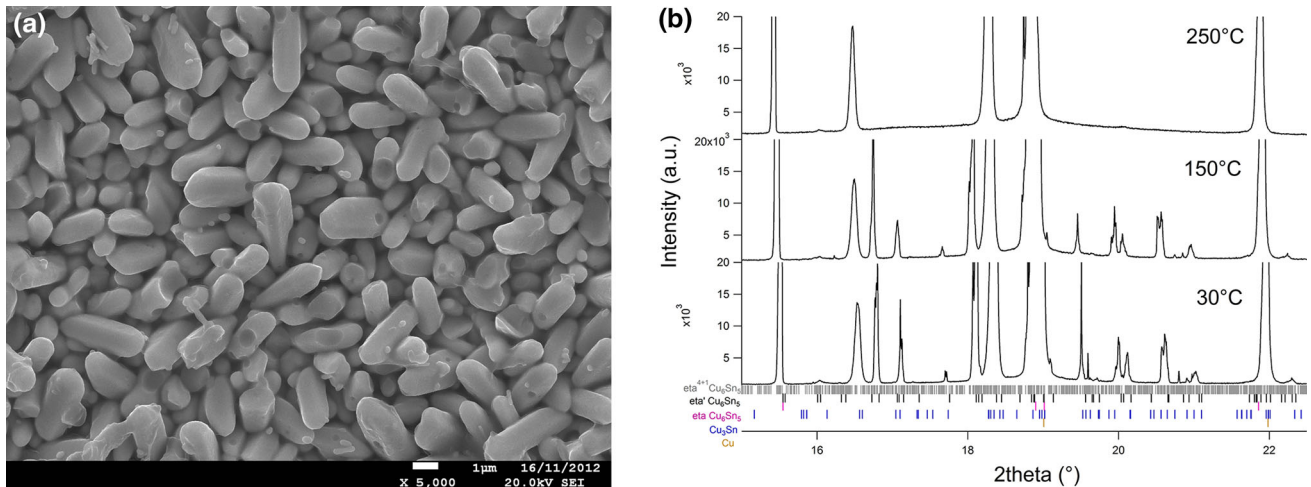


Fig. 10. (a) SEM image of the sample used for XRD, and (b) the XRD patterns from the interfacial IMCs in Sn-0.7Cu/Cu show an  $\eta'/\eta^{4+1}$   $\text{Cu}_6\text{Sn}_5$  crystal structure at 30°C and 150°C, and an  $\eta$   $\text{Cu}_6\text{Sn}_5$  structure at 250°C.

## RESULTS AND DISCUSSION

### UHV-TEM Bright Field Image of Solder Joint Cu/Cu<sub>3</sub>Sn/Cu<sub>6</sub>Sn<sub>5</sub>/Sn-0.7Cu Solder

Figure 7a and b shows a bright field image of solder joint and selected area electron diffraction from  $\text{Cu}_6\text{Sn}_5$ . Multiple small grains of a few submicron size of  $\text{Cu}_3\text{Sn}$  can be seen on the Cu substrate with a columnar morphology, with Kirkendall voids between the  $\text{Cu}_3\text{Sn}$  and the Cu substrate. It is expected that the relatively thick  $\text{Cu}_3\text{Sn}$  layer with Kirkendall voids was formed during annealing for 500 h at 150°C.<sup>20</sup> The  $\text{Cu}_6\text{Sn}_5$  layer is a typical scalloped morphology, and a single-crystal grain was observed during in situ heating experiments. According to the reported TTT diagram based on annealing for 500 h at 150°C,  $\text{Cu}_6\text{Sn}_5$  will be a stable monoclinic phase. Nevertheless, it is difficult to determine whether this monoclinic phase is  $\eta'$  or  $\eta^{4+1}$  from the electron diffraction pattern obtained from  $\text{Cu}_6\text{Sn}_5$ . The Sn phase also exists at outer areas of the  $\text{Cu}_6\text{Sn}_5$ , and interdiffusion with  $\text{Cu}_6\text{Sn}_5$  can be expected during heating in the in situ observation experiments. In Figs. 7a and 8 taken from the still-frame in situ video at 20°C, no lattice defects, such as dislocations, stacking faults, or twinning were recognized in  $\text{Cu}_6\text{Sn}_5$  grains by bright field imaging at several tilting conditions. Yet, some wide and dark-banded contrast patterns within  $\text{Cu}_6\text{Sn}_5$  were found. This contrasting is likely to be bend contours<sup>22</sup> but not thickness fringes because the sample is flat with a thickness of around 0.5  $\mu\text{m}$ , prepared by parallel ion beam milling. Note that thickness fringes only appear when the sample is not flat.<sup>22</sup>

In Fig. 8, the thick dotted lines correspond to grain boundaries of Cu,  $\text{Cu}_3\text{Sn}$ ,  $\text{Cu}_6\text{Sn}_5$ , and Sn-0.7 wt.%Cu solder, and the thin dotted lines within  $\text{Cu}_6\text{Sn}_5$  may be bend contours. Bend contours are a

diffraction phenomenon that arises from the change in orientation of particular sets of planes within the sample relative to the electron beam<sup>22</sup> and indicate that there is strain in the grains. In this instance, the patterns appear in a temperature range that is likely to correspond to the polymorphic transformation of  $\text{Cu}_6\text{Sn}_5$  and may be indicative of transformation-related stresses.

### In Situ Heating Observations from Room Temperature to 210°C

Figure 9a–h are selected still-frame TEM images from the in situ video of UHV-TEM of an interface in Cu/ $\text{Cu}_3\text{Sn}$ / $\text{Cu}_6\text{Sn}_5$ /Sn-0.7Cu solder taken at (a) 20°C, (b) 60°C, (c) 120°C, (d) 150°C, (e) 180°C, (f) 190°C, (g) 200°C, and (h) 210°C. As shown in Figs. 8 and 9a, in  $\text{Cu}_6\text{Sn}_5$ , there are contrast patterns. Note that the sample thickness is around 0.5  $\mu\text{m}$  and flat due to the FIB for parallel cutting, so the thickness fringe, if any, should be straight but not curved. Contributions from thermal expansion are estimated at approximately 1.8% volume expansion from unit cell volume measurements by synchrotron XRD.<sup>14</sup> At around 180°C, the contrast patterns moved from the left side of the  $\text{Cu}_6\text{Sn}_5$  toward the right of the  $\text{Cu}_6\text{Sn}_5$  grain, then disappeared, and finally the new contrast patterns were created from the left side of the grain. There are potentially two different monoclinic variants,  $\eta'$  and  $\eta^{4+1}$ . The former transformation temperature is reported at 186°C and the latter at 210°C. These TEM experiments involve a heating rate of 20°C/min to reach 210°C before isothermal holding. It is possible if monoclinic is  $\eta'$ , due to the relatively slow kinetics for the phase transformation from monoclinic  $\eta'$ - $\text{Cu}_6\text{Sn}_5$  to hexagonal  $\eta$ - $\text{Cu}_6\text{Sn}_5$ , a phase transformation is observed at 210°C. Or alternatively if this monoclinic variant is  $\eta^{4+1}$ , a phase transformation

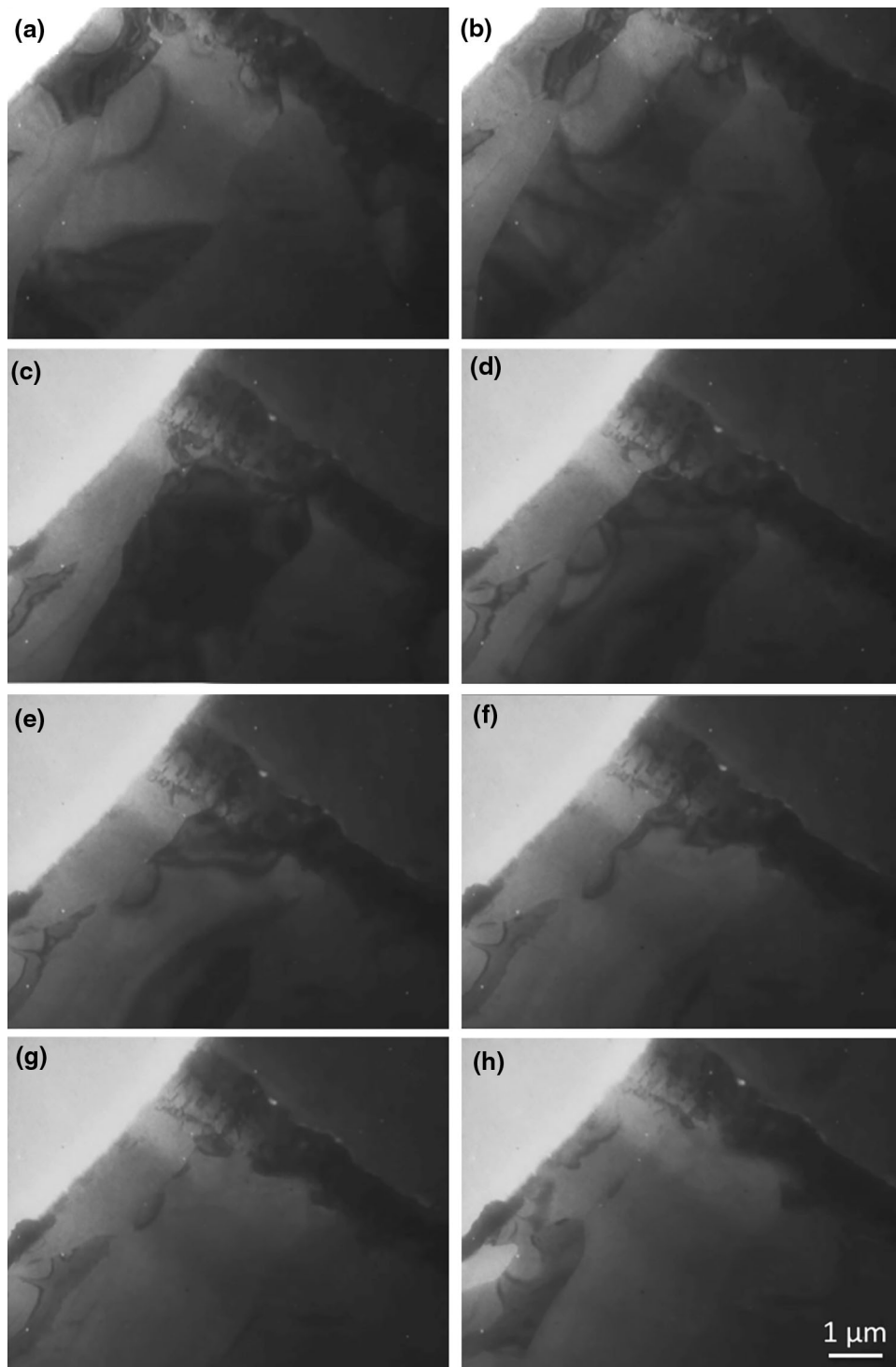


Fig. 11. Selected still-frame TEM images from in situ video of an interface in  $\text{Cu}/\text{Cu}_3\text{Sn}/\text{Cu}_6\text{Sn}_5/\text{Sn}$  taken at  $210^\circ\text{C}$  isothermally for (a) 0 s, (b) 15 s, (c) 45 s, (d) 75 s, (e) 85 s, (f) 95 s, (g) 105 s, and (h) 130 s followed by heating to  $210^\circ\text{C}$ .

occurring at  $210^\circ\text{C}$  is expected. Nevertheless, it is difficult to determine whether this monoclinic phase is  $\eta'$  or  $\eta^{4+1}$  from the electron diffraction pattern obtained from  $\text{Cu}_6\text{Sn}_5$ .

Figure 10a shows an SEM image of the sample surface after removed Sn by etching. As shown in Fig. 10b after being annealed at 500 h (identical to

TEM samples in this study), the interfacial IMCs in Sn-0.7Cu/Cu show an  $\eta'/\eta^{4+1}$   $\text{Cu}_6\text{Sn}_5$  crystal structure at  $30^\circ\text{C}$  and  $150^\circ\text{C}$  conditions. As they are heated, the peaks gradually shifted to low  $2\theta$  angle because of thermal expansion. The XRD pattern at  $250^\circ\text{C}$  became relatively flat and can be indexed as hexagonal  $\eta$   $\text{Cu}_6\text{Sn}_5$ ,  $\text{Cu}_3\text{Sn}$ , and Cu, which

indicates that polymorphic phase transformation of  $\text{Cu}_6\text{Sn}_5$  has completed. In situ XRD patterns on identical samples to the TEM study therefore revealed a polymorphic transformation of  $\text{Cu}_6\text{Sn}_5$ .

### In Situ Isothermal Observations at 210°C

To eliminate the effects of thermal expansion, isothermal in situ observations were made immediately after the temperature reached 210°C as shown in the experimental temperature profile in Fig. 6. Figure 11a–h are selected still-frame TEM images from in situ videos of the interface in  $\text{Cu}/\text{Cu}_3\text{Sn}/\text{Cu}_6\text{Sn}_5/\text{Sn}-0.7\text{Cu}$  solder taken at 210°C isothermally for (a) 0 s, (b) 15 s, (c) 45 s, (d) 75 s, (e) 85 s, (f) 95 s, (g) 105 s, and (h) 130 s followed by heating to 210°C. During early stages of the observation in Fig. 11a–d, contrast patterns moved from the grain boundary to the center of the grain. Then after 105 s in Fig. 11g, all contrast patterns disappeared. In Fig. 11g and h, there are no contrast patterns in the  $\text{Cu}_6\text{Sn}_5$ .

According to the review by Laurila et al.,<sup>23</sup> during soldering and subsequent cooling, the time available for the transformation into the low-temperature monoclinic structure is not sufficient and the high-temperature hexagonal  $\text{Cu}_6\text{Sn}_5$  remains as a metastable phase. Nevertheless, in our case, the sample had been annealed for 500 h at 150°C; the transformation to monoclinic is expected to occur, as evidenced by TTT diagram shown in Fig. 3. The expected volume change if  $\text{Cu}_6\text{Sn}_5$  transforms from the  $\eta'$ -monoclinic phase into the  $\eta$ -hexagonal phase during service is a 2.15% shrinkage based on the ambient temperature theoretical densities of monoclinic and hexagonal  $\text{Cu}_6\text{Sn}_5$ : 8.270 g/cm<sup>3</sup> and 8.448 g/cm<sup>3</sup>, respectively.<sup>24</sup> A 2% volume shrinkage would conceivably be accompanied by significant stress in the IMC layer. For our in situ experiments, no crack propagation was observed but contrast pattern formation and movement did occur. This is expected due to the sample thickness (0.5  $\mu\text{m}$ ) being insufficient to accumulate the strain for initiation of cracking.

### CONCLUSION

We observed two phenomena, namely, the polymorphic transformation of monoclinic to hexagonal  $\text{Cu}_6\text{Sn}_5$  and strain of the  $\text{Cu}_6\text{Sn}_5$  IMC layer formed at the interface of  $\text{Cu}/\text{Cu}_3\text{Sn}/\text{Cu}_6\text{Sn}_5/\text{Sn}-0.7\text{Cu}$  solder joints by in situ heating/isothermal while observing thick solder joint samples by ultrahigh-voltage transmission electron microscopy. Due to the polymorphic transformation from monoclinic to hexagonal, the strain was accumulated by volume changes that initiated at the grain boundary of the

$\text{Cu}_6\text{Sn}_5/\text{Sn}$  interface. This strain is a likely source of cracking of the  $\text{Cu}_6\text{Sn}_5$  in samples that cycle through this critical temperature range.

### ACKNOWLEDGEMENTS

This research was conducted under an international cooperative research program between the University of Queensland, Australia, Kyushu University, and Nihon Superior Company Ltd., Japan. K. Nogita was supported by the “UQ-KU Project”, which assists research collaborations between the University of Queensland and Kyushu University, during his visit at Kyushu University for high-voltage TEM experiments. PXRD experiments were performed at the Australian Synchrotron Powder Diffraction Beamline (AS132/PD/5784). The authors greatly thank Dr. Qinfen Gu of Australian Synchrotron for technical assistance.

### REFERENCES

1. M. Waldrop, *Nature* 530, 144 (2016).
2. H.-Y. Hsiao, C.-M. Liu, H.-W. Lin, T.-C. Liu, C.-L. Lu, Y.-S. Huang, C. Chen, and K.N. Tu, *Science* 336, 1007 (2012).
3. D. Mu, S.D. McDonald, J. Read, H. Huang, and K. Nogita, *Curr. Opin. Solid State Mater. Sci.* 20, 55 (2016).
4. H. Okamoto, *Phase Diagrams of Dilute Binary Alloys* (ASM International: Materials Park, OH, 2002).
5. K. Nogita, *Intermetallics* 18, 145 (2010).
6. A.-K. Larsson, L. Stenberg, and S. Lidin, *Acta Crystallogr. B* 50, 636 (1994).
7. Y.Q. Wu, J.C. Barry, J. Yamamoto, Q.F. Gu, S.D. McDonald, S. Matsumura, H. Huang, and K. Nogita, *Acta Mater.* 60, 6581 (2012).
8. K. Nogita and T. Nishimura, *Scripta Mater.* 59, 191 (2008).
9. U. Schwingenschlögl, C.D. Paola, K. Nogita, and C.M. Gourlay, *Appl. Phys. Lett.* 96, 061908 (2010).
10. K. Nogita, C.M. Gourlay, and T. Nishimura, *JOM* 61, 45 (2009).
11. K. Nogita, C.M. Gourlay, S.D. McDonald, Y.Q. Wu, J. Read, and Q.F. Gu, *Scripta Mater.* 65, 922 (2011).
12. G. Zeng, S.D. McDonald, J.J. Read, Q.F. Gu, and K. Nogita, *Acta Mater.* 69, 135 (2014).
13. D. Mu, H. Tsukamoto, H. Huang, and K. Nogita, *Mater. Sci. Forum* 654–656, 2450 (2010).
14. D. Mu, J. Read, Y.-F. Yang, and K. Nogita, *J. Mater. Res.* 26, 2660 (2011).
15. D. Mu, H. Huang, and K. Nogita, *Mater. Lett.* 86, 46 (2012).
16. H. Tsukamoto, T. Nishimura, and K. Nogita, *Mater. Lett.* 63, 2687 (2009).
17. D. Mu, H. Yasuda, H. Huang, and K. Nogita, *J. Alloys Compd.* 536, 38 (2012).
18. D. Mu, H. Huang, S.D. McDonald, and K. Nogita, *J. Electron. Mater.* 42, 304 (2013).
19. D. Mu, H. Huang, S.D. McDonald, J. Read, and K. Nogita, *Mater. Sci. Eng. A* 566, 126 (2013).
20. G. Zeng, S.D. McDonald, Q.F. Gu, Y. Terada, K. Uesugi, H. Yasuda, and K. Nogita, *Acta Mater.* 83, 357 (2015).
21. R.W. Cheary and A. Coelho, *J. Appl. Crystallogr.* 25, 109 (1992).
22. E.A. Stach, T. Freeman, A.M. Minor, D.K. Owen, J. Cummings, M.A. Wall, T. Chraska, R. Hull, J.J.W. Morris, A. Zettl, and U. Dahmen, *Microsc. Microanal.* 7, 507 (2001).
23. T. Laurila, V. Vuorinen, and J.K. Kivilahti, *Mater. Sci. Eng. R* 49, 1 (2005).
24. G. Ghosh and M. Asta, *J. Mater. Res.* 20, 3102 (2005).